Continuous-Wave 3.1–3.6 μm Difference-Frequency Generation of Dual Wavelength-Tunable Fiber Sources in PPMgLN-Based Rapid-Tuning Design

Junqing Zhao, Fuqiang Jia, Yutong Feng, and Johan Nilsson

***Abstract*—We report on a single-frequency continuous wave (CW) difference-frequency generation (DFG) source based on single-frequency wavelength-tunable polarization-maintaining ytterbium- and erbium-doped fiber master oscillator–power amplifiers (MOPAs), acting as the pump and signal source, respectively, and a 40-mm long periodically poled MgO-doped $LiNbO_3$ (PPMgLN) crystal. Owing to the dual wavelength-tuning of the MOPAs, the generated idler light reaches a wavelength-tuning range of close to 500 nm, from ∼3117.2 to ∼3598.8 nm, only by tuning the launched pump and signal wavelengths from 1040 to 1084.6 nm and from 1545.2 to 1561.4 nm, respectively, without any change of temperature or grating period of the PPMgLN. Compared to temperature-based idler-wavelength-tuning, this method is potentially faster in speed. The maximum idler power exceeds 60 mW, which is the highest reported power for a wavelength-tunable single-frequency CW DFG source. A rapidly wideband-tunable DFG source with tens of milliwatts of output power in a narrow line can be a practical tool for mid-infrared molecular spectroscopy, detection, and sensing at high measurement rates.**

***Index Terms*—Doped fiber amplifiers, nonlinear optics, optical mixing.**

I. Introduction

TUNABLE mid-infrared (MIR) coherent sources are widely utilized for molecular detection, absorption spectroscopy, and gas remote sensing [1]–[5]. Optical parametric oscillator (OPO) [6]–[10] and difference-frequency generation (DFG) sources [1]–[5] are well-established options for this, both of which are based on nonlinear frequency conversion in nonlinear crystals such as periodically poled lithium niobate (PPLN) [1], magnesium-doped PPLN (PPMgLN) [7]–[10], and zinc germanium phosphide (ZGP) [11]. Both OPOs and DFG sources rely on parametric down-conversion of pump radiation into signal and idler radiation, where the idler radiation is typically the sought-after MIR radiation. Whereas an OPO is driven only by the pump, a DFG source requires additional driving by another input wave. This is typically the signal, and the idler is then generated through nonlinear wave-mixing. Both OPOs and DFGs require phase-matching for efficient conversion. Although the phase-matching bandwidth is typically only of the order of 1 nm or less, wideband wavelength-tuning of DFGs can be realized by tuning two parameters simultaneously, in a manner which changes the idler wavelength for which phase-matching is achieved. The tuning parameters can be the pump wavelength, signal wavelength, crystal temperature, crystal angle, and grating period (at least one wavelength must be changed together with at least one more parameter, which may be the other driving wavelength.) Even if DFGs are normally less efficient than OPOs and require both pump and signal input, they nevertheless offer important attractions. DFG is typically a single-pass process that allows for simple cavity-free configurations. Furthermore it is possible to control the linewidth of the MIR idler by controlling the linewidth of the pump and signal light, so injection-locking or intracavity filtering is not necessary [12], [13]. In addition, the pump and signal are often at readily available wavelengths in the near-infrared, so in contrast to an optical parametric amplifier (OPA) [14] for the MIR, it is not necessary to seed the conversion at the desired MIR wavelength.

Many PPLN- or PPMgLN-based tunable DFG sources and related applications have been demonstrated in the last two decades in the low-power regime, where the conversion efficiency is not so critical. The first wavelength-tunable bulk DFG source was demonstrated by Goldberg *et al*. [15]. They used a PPLN crystal driven by a 1064-nm Nd:YAG signal laser and a 750–950-nm tunable Ti:Al_2O_3 pump laser to generate 3.0–4.1-μm MIR radiation. The phase-matching was tuned by rotation of the PPLN crystal. Maddaloni *et al*. demonstrated a 3.5-mW PPLN-based CW DFG source and used it for sub-Doppler molecular spectroscopy [1]. They obtained a tuning range of 2.9–3.5 μm by tuning the temperature between 50 and 68 °C. Armstrong *et al*. also achieved temperature-based wavelength tuning, between 3378 and 3458 nm, though the power level of their DFG source was limited to a few microwatts [2]. Høgstedt *et al*. demonstrated a tunable CW DFG source with 3.06-mW maximum power at 3.03 μm [3]. Their 500 nm tuning range resulted from shifts between four different grating periods together with adjustments of crystal temperature and pump wavelength. Mao *et al*. demonstrated a 3.1 to 3.6 μm tunable CW DFG source realized by simultaneously tuning the grating period, temperature, and signal wavelength [16]. This wavelength range is attractive for the detection of several species through the H-C stretch vibration and fortuitously, can be reached by DFG

Manuscript received March 15, 2017; revised May 28, 2017; accepted July 5, 2017. This work was supported by EPSRC through the FLITES program (EP/J00278X/1). *(Corresponding author: Yutong Feng.)*

The authors are with the Optoelectronics Research Centre, University of Southampton, Southampton SO17 1BJ, U.K (e-mail: junqingzhao@outlook.com; jiafq@xmu.edu.cn; Y.Feng@soton.ac.uk; jn@orc.soton.ac.uk).

Color versions of one or more of the figures in this paper are available online at http://ieeexplore.ieee.org.

Digital Object Identifier 10.1109/JSTQE.2017.2725442

between 1–1.1 μm and 1.5–1.6 μm, where excellent fiber-based sources have been demonstrated.

Although these and other demonstrated DFG sources were widely tunable, they relied on tuning of the temperature-tuning and/or the grating period. Those approaches are relatively slow, and it may take several minutes for the temperature to be fully stabilized after each adjustment. This makes them less suitable for applications that require fast tuning.

The demonstrated power levels are also inadequate for some applications. However, a PPMgLN-based DFG source driven by an Yb-doped fiber source at 1.064 μm and an Er-doped fiber source at 1.550 μm has recently been scaled to 3.55 W of output power at 3.4 μm [17]. This was driven by sources with relatively large linewidths and was not tunable, but it still suggests that considerably higher MIR output powers are possible also from tunable DFG sources with the sophistication required for high-resolution molecular spectroscopy.

In this paper, we report a single-frequency CW DFG source that can be wavelength-tuned by simultaneously tuning the pump and signal wavelength, without any change of the crystal temperature, angle, or grating period. We obtain a wavelength tuning range from ~3117.2 to ~3598.8 nm, i.e., nearly 500 nm. The pump source is a single-frequency Yb-doped fiber MOPA (master oscillator–power amplifier) seeded by a diode laser (DL) tunable around 1060 nm, and the signal source is a single-frequency Er-doped fiber MOPA seeded by a diode laser tunable around 1550 nm. Although the 1060-nm diode laser was tuned manually and therefore only slowly, it is possible to replace our seed lasers with fast-tuning versions. Alternatively, if diode-switching is used instead of tuning, nanosecond-level wavelength-switching is possible. We further take advantage of the excellent efficiency and power scalability of fiber MOPAs in potentially low-cost and robust implementations to offset the low efficiency of CW DFG and scale the idler power to over 60 mW. In combination with high power, the potential for fast switching and simple robust implementations opens up for fast measurements in harsh environments, e.g., for large-scale species-selective MIR tomography at high frame rates such as required for measurements on aero-engines [18]–[22].

II. Experimental Configuration

The DFG setup is schematically shown in Fig. 1. The main parts are the pump and signal MOPA systems and a PPMgLN crystal. All lightwaves are linearly polarized, and both amplification systems employ polarization-maintaining fibers throughout. They are both seeded by external-cavity DLs operating on a single longitudinal mode. The seed lasers and all amplifiers are separated by isolators. The output beams from the two MOPAs are then combined and co-coupled into the PPMgLN crystal to produce idler radiation through DFG. Preliminary studies suggested that a signal wavelength around 1550 nm and a pump wavelength around 1060 nm would maximize the MIR tunability in the range 3.1–3.6 μm, and the MOPAs therefore targeted maximum tunability around those wavelengths.

The signal-MOPA system comprises a seed laser (Agilent 8164A) with a linewidth specified to less than 100 kHz and

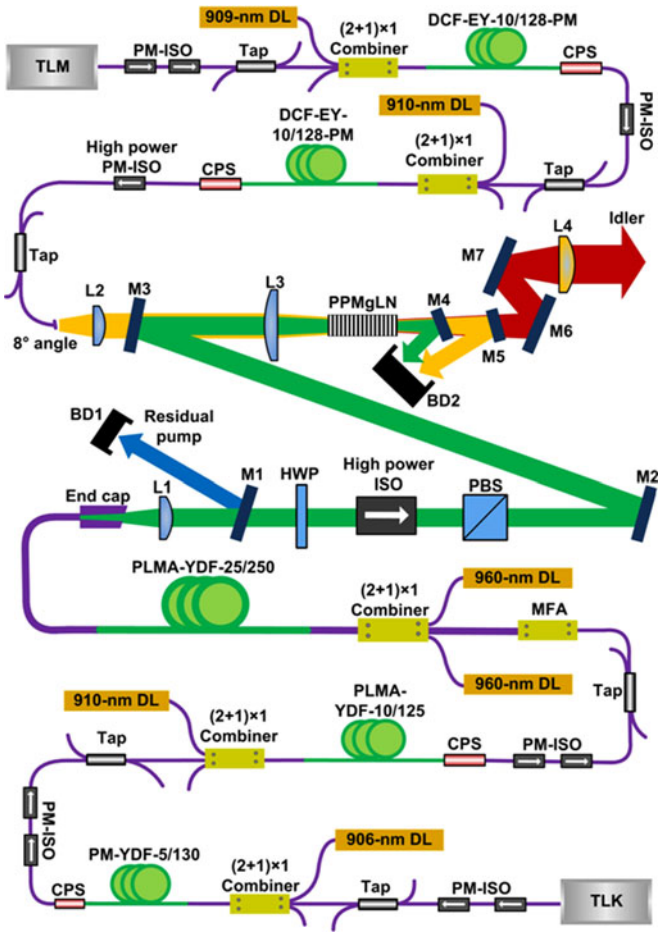

Fig. 1. Schematic of experimental setup. TLK: tunable laser kit; PM-ISO: polarization-maintaining isolator; Tap: 1:99 tap coupler; DL: diode laser; PM-YDF: polarization-maintaining ytterbium-doped double-clad fiber; PLMA: polarization-maintaining large mode area; CPS: cladding power stripper; MFA: mode-field adapter; BD: beam dump; L1-L4: different lenses; M1-M7: different mirrors; HWP: half wave plate; PBS: polarizing beam splitter cube; TLM: tunable laser module; DCF-EY: erbium-ytterbium co-doped double-clad fiber.

a tuning range of 1510–1640 nm. This is followed by two Er:Yb co-doped fiber amplifiers comprising approximately 3-m lengths of the same gain fiber, CorActive DCF-EY-10/128-PM. The length influences the gain bandwidth of fiber amplifiers with reabsorption [23]. This determined the gain fiber lengths to 3 m in the 1st amplifier and 2.8 m in the 2nd amplifier. A shorter gain fiber counteracts the reabsorption-induced shift of the gain peak to longer wavelengths in the more strongly saturated second amplifier. The fiber has a core diameter of 9.3 μm, cladding diameter of 128 μm, cladding-absorption of 2.0 dB/m at 915 nm, and core-absorption of 99 dB/m at 1535 nm. Both fibers are pumped by fiber-coupled DLs at 0.91 μm. The MOPA also includes taps for monitoring of light in the forward and backward direction (e.g., stimulated Brillouin scattering, SBS), as well as isolators, as illustrated in Fig. 1. It can reach ~5.0 W of output power, after a fiberized isolator spliced to the output of the 2nd amplifier.

The pump-MOPA system comprises a Littman-configured Thorlabs TLK-1050M seed laser followed by three cascaded cladding-pumped ytterbium-doped amplifiers (YDFAs). All

ytterbium-doped fibers (YDFs) possess Yb:aluminosilicate-like spectral characteristics. Analogously to the signal MOPA, the length of all the YDFs were chosen to provide a suitable tuning range, since the achievable gain bandwidth is largely determined by the laser dopant's concentration–length product. Importantly, the pump absorption also depends on the fiber length as well as on the pump wavelength. This can lead to conflicting length requirements. Insofar as possible and deemed necessary, we resolved such conflicts by adjusting the pump wavelength to yield appropriate pump absorption in the different stages.

The 1st-stage amplifier utilizes ~3.7-m of gain fiber (Nufern, PM-YDF-5/130-VIII), with mode field diameter (MFD) of ~6.1 μm at 1060 nm, cladding diameter of 130 μm, and cladding absorption of 0.61 dB/m at the secondary peak at ~915 nm. It is cladding-pumped by a 906-nm DL with 2.5 W maximum power from a conventional 105-μm-core fiber pigtail. This is launched into the YDF via a $(2 + 1) \times 1$ pump/signal combiner. After the YDF, an in-house cladding-power-stripper (CPS) strips the residual pump light. Although the seed laser is tunable from 991 to 1087 nm, the gain bandwidth of the 1st YDFA is limited to 1030–1085 nm. With a similar structure, the 2nd amplifier utilizes ~3.2 m of gain fiber (Nufern, PLMA-YDF-10/125-VIII), which is cladding-pumped by a 910 nm DL with up to 12.4-W output power, again from a 105-μm-core fiber pigtail. The inner-cladding/core area ratio is smaller in this fiber, which increases the pump absorption for a specific spectral range and level of the gain.

The 3rd-stage main power amplifier uses ~3.7-m of gain fiber (Nufern, PLMA-YDF-25/250-VIII) with cladding absorption of 1.8 dB/m at the secondary peak at ~915 nm, core diameter of 26.2 μm and cladding diameter of 254 μm. A fiber-taper-based mode field adapter (MFA) reduces the coupling loss from the much-smaller core in the 2nd YDFA to less than 0.5 dB. Two 960-nm DLs, each with maximum output power of ~60 W from a 105-μm-core fiber pigtail, are utilized for pumping. Furthermore, we utilize two fiber-pigtailed isolators before each amplifier to achieve wideband high isolation, and 1% tap couplers to monitor any backward light induced, e.g., by SBS or reflections. A matched piece of 25/250 passive fiber is spliced to the output of the 3rd YDF together with an end-cap to reduce the power density at the air/silica interface via beam expansion and to reduce the coupling of Fresnel-reflected light back into the fiber core. The pump MOPA can reach ~55.1 W of output power.

The pump beam from the Yb MOPA is expanded and delivered through the end-cap, and then collimated by an aspheric lens with focal length (FL) of 26 mm. A dichroic mirror (M1), highly reflective (HR) at 800–980 nm and highly transmissive (HT) at 1030–1600 nm, reflects the unabsorbed 960-nm light into a beam dump (BD1). The pump beam is then launched through a half-wave plate (HWP) and a free-space isolator. Note that although the isolator is of the polarization-independent type, the small but uncontrolled difference in the optical path length of its linearly polarized eigenstates means that it does not in general preserve the polarization. Thus, in order to maintain the linear polarization, we identified the principal axes of the isolator and adjusted the polarization to one of them. Furthermore, the PPMgLN crystal requires that the launched light should be e-polarized, i.e., with polarization perpendicular to the crystal plane (so vertical). Therefore the isolator was rotated to ensure that the output linear polarization, on a principal axis of the isolator, was vertical. The HWP was then adjusted to align the polarization to the appropriate principal axis on the input of the isolator. A polarizing beam splitter (PBS) cube after the isolator removes any residual horizontally polarized light to ensure only e-polarized light can be coupled into the PPMgLN crystal. The pump beam is then reflected in mirror M2 with an angle of incidence of ~10°, and further combined with the beam from the signal-MOPA in the dichroic mirror M3.

The signal polarization is adjusted by rotating the end of the signal MOPA's PM output fiber. The output is then collimated in a lens L2 with 25 mm FL. Following beam combination in M3, a lens (L3) with FL of ~100 mm is used to couple both beams into the PPMgLN crystal (Covesion, MOPO1-1.0-40). This is 40-mm long and is mounted on a clip in a temperature-controlled oven. Two CaF_2 mirrors, M4 and M5, block the unconverted pump and signal light, respectively. The idler beam is then height-adjusted by two steering mirrors (M6 and M7) to match the aperture of a spectrum analyzer (Bristol 721). A CaF_2 lens AR-coated from 3 to 5 μm (L4) collimates the idler beam.

III. Characteristics of the Pump and Signal MOPAs

The output power from the 1st YDF amplifier reaches 128–206 mW, depending on the wavelength within the 1030–1085-nm range. The power is reduced to 64–153 mW at the input of the 2nd YDF by inter-stage losses in the isolators, tap coupler, pump combiner, and splices. The 2nd amplifier boosts the power to 3.31–3.53 W in the range 1030–1085 nm, which drops to 0.81–1.2 W at the input of the 3rd YDF due to losses in components and splices.

Fig. 2 shows the output characteristics of the 3rd (final) amplifier when its total pump power is 96.7 W. Fig. 2(a) depicts spectra measured with a resolution of 0.1 nm. The usable tuning range reduces to 1038–1085 nm, limited by parasitic amplified spontaneous emission (ASE) at the gain peak at ~1070 nm. Gain peaking and the concomitant reduction in tuning range becomes more severe as the gain and thus gain differences build up along the amplifier cascade. Thus, for operation in the short edge ~1038 nm for instance, the peak gain becomes significantly higher than the 1038-nm laser-gain. This leads to strong ASE at the gain peak. The ASE dominates the output, whereas the laser power fraction becomes as low as ~23.9%, calculated by spectral integration. By contrast, for operation at 1072 nm, the laser-gain is similar to the peak gain, so the laser power fraction can reach ~99.7%. The dependence of the total output power (including ASE) as well as the useful laser output power on the tuning wavelength is plotted in Fig. 2(b). The total output power (including both laser and ASE) is relatively constant across the tuning range, which is expected. However, the tuning leads to clear variations in the useful laser power, The inset of Fig. 2(b) also shows a typical 2D power distribution, at 1064 nm as reconstructed by a beam profiler (Thorlabs BP104-IR) from the 1D distributions it measured in orthogonal

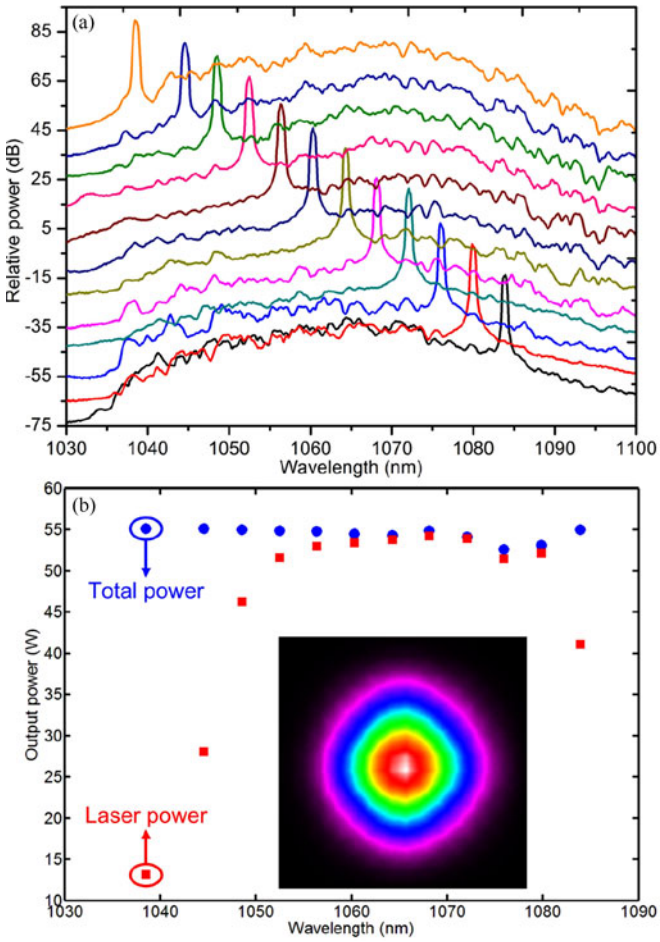

Fig. 2. Output characteristics from the Yb MOPA. (a) Spectra for laser wavelengths of 1038–1084 nm measured with resolution of 0.1 nm. The spectra are offset in steps of 10 dB for clarity. (b) Total output power including ASE (upper blue circles) and laser output power (lower red squares) against tuning wavelength; Inset: Typical reconstructed 2D laser output beam profile.

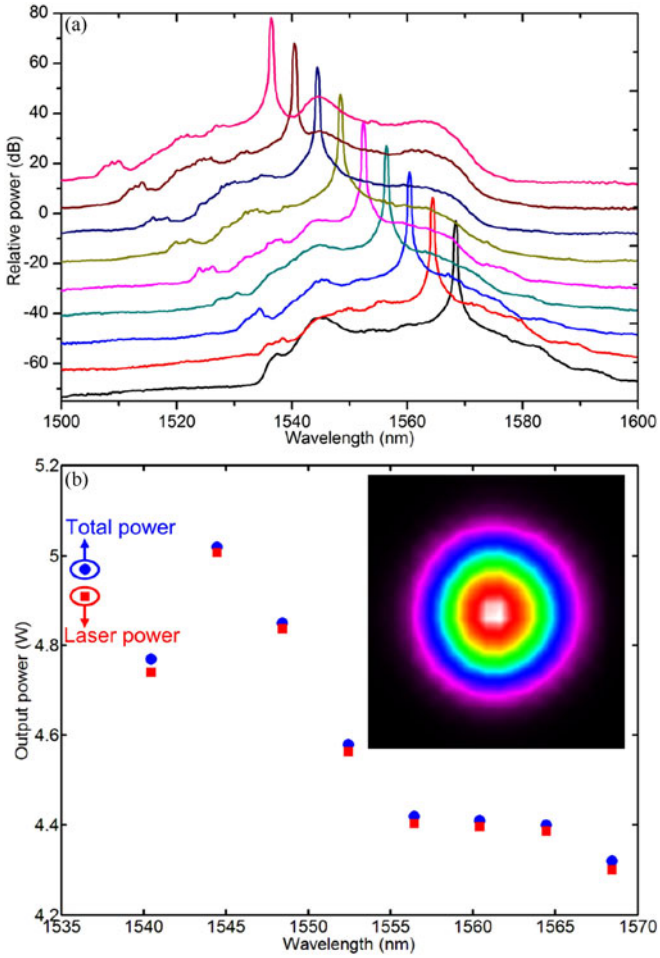

Fig. 3. Output characteristics from the Er MOPA. (a) Spectra for laser wavelengths of 1536–1568 nm measured with resolution of 0.1 nm. The spectra are offset in steps of 10 dB for clarity. (b) Total output power including ASE (upper blue circles) and laser output power (lower red squares) against tuning wavelength; Inset: Typical reconstructed 2D laser output beam profile.

transverse directions. The beam profiler also gives an M^2-factor of $\sim$1.23. The laser beam profile depended only weakly on the wavelength and the M^2 factor varied between 1.23 and 1.39 across the Yb-MOPA wavelength range, at full power. The use of a multimode gain fiber in the 3rd stage ($V = 4.6$) may have degraded the beam quality from the ideal value of $M^2 = 1$. Thermal effects in the gain fiber as well as in the output isolator can also degrade the beam quality.

There is no noticeable backward light in any of the tap couplers, suggesting that no SBS occurs in the pump-MOPA.

In the signal-MOPA, the 1st amplifier boosts the laser power of 1.66–1.91 mW from the seed-DL to 76.8–117 mW within the wavelength range of 1536–1568 nm when using $\sim$1.82 W of pump power at 909 nm. When pumped by $\sim$22.7 W, the output power from the 2nd amplifier reaches 4.32–5.02 W. We did not measure the pump leakage, but the fiber parameters suggest this is significant. Increasing the fiber length is undesirable insofar as it degrades the tuning range. Instead, the absorption can be improved by pumping at the absorption peak at 975 nm, which may then improve the efficiency. Fig. 3 plots output spectra and power distributions for seed-laser wavelengths of 1536–1568 nm. Although the tuning range is limited by the amplifiers also for this MOPA, the ASE is much lower, suggesting that the tuning could be expanded. The laser power has also been plotted for each wavelength, as seen in Fig. 3(b). A typical 2D beam profile as reconstructed from 1-D measurements can be seen in the inset of Fig. 2(b). The M^2 factor is measured to be $\sim$1.01. In the same manner as for the pump-MOPA, the beam profile remains essentially unchanged within the 1536–1568-nm range; the M^2 factor varies between 1.01 and 1.05.

IV. Difference Frequency Generation and Discussion

After precisely collimating and combining the pump and signal beams, we use lens L3 to launch them into the PPMgLN crystal. The system is carefully aligned to create a common focus, close to the center of the PPMgLN crystal, with similar spot sizes. The signal spot diameter at focus was 105 μm and varied by $\sim$1 μm in the 1536–1568 nm range. For the pump, the focused spot diameter was 109 μm and varied by $\sim$2 μm in the 1038–1085 nm range. These were measured in air but the spot sizes at focus are not expected to change when the PPMgLN

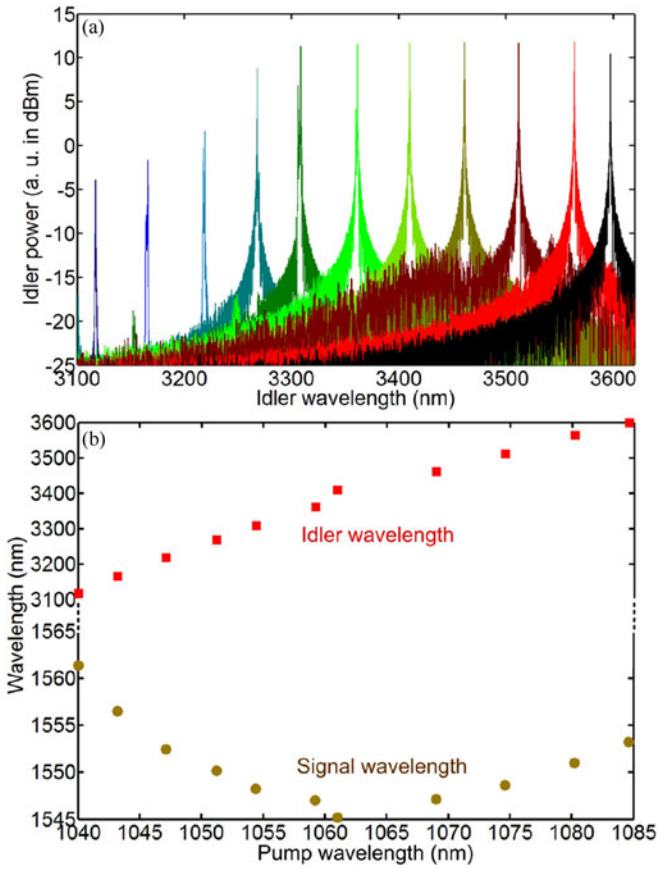

Fig. 4. (a) Generated idler spectra (minimum resolution ~0.1 nm) for different idler wavelengths; (b) Relations between signal, idler and pump wavelengths.

crystal is inserted into the beam. During wavelength tuning, the separation between the foci of the two beams is always <0.8 mm, as measured in air. The Rayleigh lengths for the signal and pump beams, inside the crystal, are estimated to be around 12 and 15 mm, respectively. Although the beam characteristics are measured in air, the pump and signal laser beams should be able to overlap well around focus also inside the PPMgLN crystal.

The PPMgLN crystal contains five separate poled gratings with different periods, 29.52, 29.98, 30.49, 31.02 and 31.59 μm, each with aperture of $1 \times 1\,\text{mm}^2$. Here we choose the grating period of 29.98 μm and set the operating temperature to 160 °C, which allows for phase-matching over a large fraction of the tuning wavelength ranges of the pump and signal MOPAs. Fig. 4(a) shows output idler spectra from the DFG system for different idler wavelengths. The idler wavelength shifts from 3117.2 to 3598.8 nm as the pump wavelength increases from 1040 to 1084.6 nm; meanwhile, we tune the signal wavelength between 1545.2 and 1561.4 nm to maintain phase-matching. We emphasize that no other parameters changed during this tuning of the idler wavelength. The idler wavelength range agrees well with H-C stretch absorption features expected from unburnt hydrocarbons in aero-engine exhaust plumes.

Fig. 4(b) gives the experimentally determined pump, signal, and idler wavelengths. These must satisfy the grating-assisted phase-matching condition, i. e.,

$$\begin{cases} 1/\lambda_p - 1/\lambda_s = 1/\lambda_i, \\ n_p/\lambda_p - n_s/\lambda_s - 1/\Lambda_g = n_i/\lambda_i. \end{cases} \tag{1}$$

Here $\lambda_{p,s,i}$ represent the pump, signal and idler wavelength, respectively, and $n_{p,s,i}$ the refractive index in the PPMgLN. Λ_g is the grating period. Fig. 4(b) confirms that the signal wavelengths required for the tuning range we achieved are well within the 1536–1568 nm tuning range of the signal MOPA. Thus, the idler wavelength range is primarily limited by the pump tuning range. As noted in Section III, the pump tuning is in turn limited by gain peaking. A gain-flattening filters or narrow-band filters which co-tune with the seed laser could be used to counteract this and the buildup of parasitic ASE, and thus increase the pump tuning range beyond the 37 nm we reached. It may also be possible to widen the pump tuning range by further optimizing the concentration–length product of the gain fibers. Yb-doped fibers can amplify from 975 nm to well over 1100 nm, and a tuning range of 144 nm was achieved by Royon *et al*. in an Yb-doped fiber laser [24]. However, a laser can operate at low gain. By contrast, in an amplifier, the substantial gain variations and gain peaking that results from the combination of reabsorption and homogeneous gain broadening limits the wavelength range over which high gain can be achieved. Still, we estimate that it may be possible to reach 10–15 dB of gain over more than 80 nm in an YDFA. A wider tuning range is likely to require additional cascaded amplifiers with lower gain and additional spectral filtering. It may also be possible to use parallel gain fibers in the architecture used to extend the gain bandwidth of erbium-doped fiber amplifiers tor telecommunications [25]. However this approach seems doubtful for high-power MOPAs,

We also note that if we also change the temperature and/or grating period of the crystal, the maximum idler tuning range as limited by the tuning ranges of our fiber MOPAs extends from $(1038\,\text{nm})^{-1} - (1568\,\text{nm})^{-1} = (3071\,\text{nm})^{-1}$ to $(1085\,\text{nm})^{-1} - (1536\,\text{nm})^{-1} = (3695\,\text{nm})^{-1}$. This is not much more than what we achieved without any change of grating period or temperature.

Fig. 5(a) depicts the output idler power and the corresponding conversion efficiency against the generated idler wavelength. Here, the conversion efficiency η refers to

$$\eta = P_i/P_s \cdot P_p \tag{2}$$

where P_i, P_s, P_p are the idler, signal and pump powers, respectively. This conversion efficiency can be viewed as a figure-of-merit. Within the underlying undepleted-wave approximation, it does not depend on the power of the signal and idler beams, although it does depend on the beam quality and focusing arrangement as well as on the spectral characteristics. Fig. 5(a) and Fig. 4(a) show that the output idler becomes much weaker on the long and short wavelength sides compared with the central region. This is mainly caused by the strong ASE (Fig. 2(a)) and associated reduction in useful pump power (Fig. 2(b)) when operating at the gain edges of the Yb-MOPA,. The highest idler power of ~62.4 mW is achieved at an idler wavelength of ~3563.6 nm with incident pump and signal laser power of ~23.2 and ~4.31 W, respectively. If we compensate for the

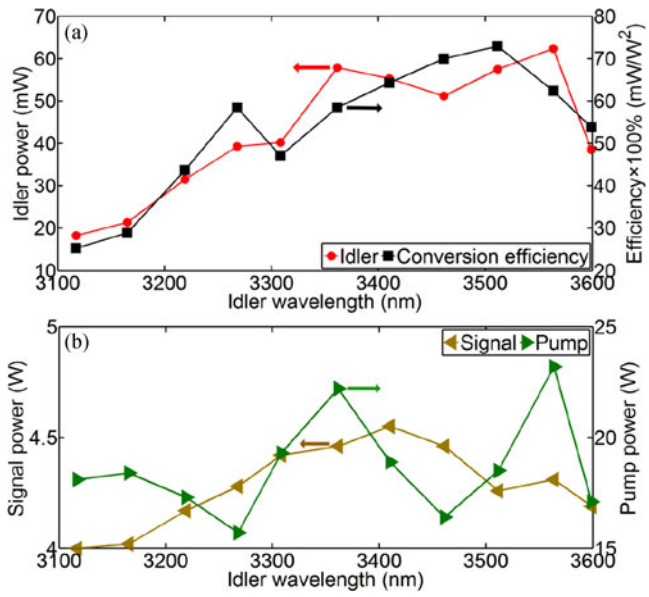

Fig. 5. (a) Output idler power and the corresponding conversion efficiency as a function of idler wavelength and (b) corresponding signal and pump power launched into the PPMgLN crystal.

20% loss of idler power we estimate in the output optics, the idler power out from the PPMgLN-crystal becomes 78.0 mW. The highest idler output power also corresponds to the highest conversion efficiency of 0.91 mW/W^2 out from the crystal.

Fig. 5(b) further gives the total powers from the pump and signal MOPAs, recorded prior to the PPMgLN crystal, for each idler wavelength. The e-polarized pump power launched into the PPMgLN crystal fluctuates significantly against wavelength. This is largely caused by the fiber-pigtailed PM isolators between the 2nd and 3rd amplifier stages of the Yb-MOPA. Both isolators have strong wavelength-dependent insertion losses. Less power fluctuations are expected with isolators with reduced wavelength-dependence.

The conversion efficiency of DFG is often quite low, especially in the CW regime [26]. Although the power levels we achieved are adequate for many applications, we were still only able to convert around 1% of the pump photons. We next consider the scope for improvements in efficiency and output power of our DFG system. This is possible with longer crystals, better focusing, better beam quality (including polarization and spectral purity), and/or higher driving power.

According to [1], it is possible to achieve a conversion efficiency which scales with the crystal length according to the following approximate expression:

$$\eta = L \times k,\ \mathrm{mW/W^2}, \tag{3}$$

Here, k is a constant in the range 0.3–0.4 cm^{-1} [27]. The precise efficiency depends on the interacting wavelengths and furthermore, this is in the absence of pump depletion, which is often negligible in DFG. Ref. [27] also recommends a confocal focusing arrangement. However, according to more precise equations [28] for the undepleted-pump regime, tighter focusing can improve on confocal focusing, e.g., by 14% in [17]. There, in a 50-mm long PPMgLN, a length-normalized conversion efficiency of 0.59 mW/W^2/cm was possible according to simulations, and 0.53 mW/W^2/cm was obtained experimentally. Similar prediction have also been verified theoretically by Boyd *et al*. [29]. According to their calculations, the optimum focusing parameter is given by

$$\xi = l/b = 2.84, \tag{4}$$

where l is the crystal length and b is the confocal parameter (twice the Rayleigh length). For confocal focusing, $\xi = 1$. For our case, the focusing parameters for the signal and pump beams are 1.67 and 1.33, respectively, whereas the values in [17] are 2.5 and 2.3, respectively. Thus, our conversion efficiency may improve with tighter focusing, beyond the length-normalized value of 0.23 mW/W^2/cm that we achieved. Experimental limitations and damage concerns prevented us from fully optimizing the focusing. Still, according to [17], the dependence of the conversion efficiency on the waist size is relatively weak around the optimum, so our looser focusing seems unlikely to fully explain our lower conversion efficiency. Alternatively, impaired beam quality or polarization may have degraded our conversion efficiency. Regardless, the higher conversion efficiency in [17] would more than double the MIR output power.

Equation (2) can be rewritten as $P_i = \eta\, P_s\, P_p$. According to this formula, for a fixed total pump + signal power, the highest idler power is obtained for equal pump and signal power. Still, the higher power efficiency of Yb MOPAs suggests that the overall efficiency will be higher if the Yb-MOPA power is higher than that of the Er-MOPA. However, a power-imbalance with higher pump power is bad from a damage point-of-view. Note here that (4) is only relevant for powers for which damage can be avoided. Looser focusing allows for higher powers. Insofar as they are available, higher powers will readily compensate for the small reduction in η at, e.g., confocal focusing. Confocal focusing (with $\xi = 1$) allows for 2.84 times more power than the lower-power optimum of $\xi = 2.84$ for the same intensity at focus. Specifically. with confocal focusing in a 40-mm crystal, the spot areas at focus become ~10,000 μm^2 at 1060 nm and ~15,000 μm^2 at 1550 nm. The maximum power density of 500 kW/ cm^2 = 5 mW/μm^2, as recommended by the manufacturer [27], is then reached for 30 W each of pump and signal. The simple conversion formula then suggests that a power of up to 0.4 mW/ W^2/cm $\times$ 30 W $\times$ 30 W $\times$ 4 cm = 1.44 W is possible. Then, ~16% of the pump photons would be converted. The pump depletion may be significant and could reduce the rate of conversion to the idler. However, the signal power grows at the same time, so the overall impact on the conversion efficiency may be small. The required increase of power from the Er-MOPA may be achieved by adding a third amplifier with a larger core. For example, 150 W of unpolarized output power has been reached in the single-frequency regime with a core diameter of 30 μm [30]. From the beam parameter, we estimate that [17] used a power density at focus of ~1470 kW/cm^2. This value is approximately 4.9 times the supplier-recommended damage threshold of the PPMgLN crystal we utilized. By contrast, we kept the combined power density inside the crystal at 300 kW/cm^2, which by some margin complies with the PPMgLN supplier's recommendation. Thus,

although we could reach 55 W of pump power and presumably reach higher conversion efficiency, we refrained from using this power for fear of damaging the crystal, e.g., through the photorefractive effect [27].

Further power-scaling is possible with an increased interaction length. Crystal lengths of 80 mm are commercially available [31]. With the same 30-W MOPAs, this can double the idler power compared to a 40-mm crystal. Furthermore, since the beam areas are proportional to the crystal length with confocal focusing (and more generally with constant ξ), it is possible to double the MOPA power to 60 W, within a 500 kW/cm^2 damage limit, and conceivably reach exceptional conversion efficiencies and idler power of over 10 W. Our current work on a 2-μm system for CO_2 imaging suggests that such power levels are adequate for species-selective tomography on aero-engines [18]–[20]. Otherwise, if a CW idler is not required, pulsed pumping is an alternative way to improve the conversion efficiency and reach watt-level idler power [32], [33].

V. Conclusion

To conclude, we have demonstrated a CW MIR single-frequency DFG source tunable from 3.1 to 3.6 μm. This is based on two wavelength-tunable single-frequency PM fiber MOPAs and a 40-mm PPMgLN crystal. The wavelength tunability is achieved by solely tuning the pump and signal wavelengths, without any change of the temperature or the grating period, which can potentially quicken the wavelength-tuning compared with typical temperature-based tuning method, with only a small compromise in tuning range. The achieved maximum idler output power can reach ~62.4 mW at ~3563.6 nm with incident pump and signal laser power of ~23.2 and ~4.31 W, respectively, corresponding to a DFG conversion efficiency of 0.91 mW/W^2. Such a wideband-tunable CW MIR source with tens of milliwatts of output power can be a practical tool for species-selective tomography on aero-engines. It can also be utilized for other MIR molecular spectroscopy, detection and sensing applications, especially when high measurement rates as enabled by high power and fast wavelength tuning are required.

Acknowledgment

The authors would like to thank Dr. L. Xu and Prof. A. Peacock in the ORC for lending the mid-infrared components and spectrum analyzer, respectively. All data supporting this study are openly available from the University of Southampton repository at http://doi.org/10.5258/SOTON/D0024.

References

[1] P. Maddaloni, G. Gagliardi, P. Malara, and P. De Natale, "A 3.5-mW continuous-wave difference-frequency source around 3 μm for sub-doppler molecular spectroscopy," *Appl. Phys. B*, vol. 80, no. 2, pp. 141–145, 2005.

[2] I. Armstrong *et al.*, "Detection of CH4 in the mid-IR using difference frequency generation with tunable diode laser spectroscopy," *J. Lightw. Technol.*, vol. 28, no. 10, pp. 1435–1442, May 2010.

[3] L. Høgstedt, O. B. Jensen, J. S. Dam, C. Pedersen, and P. Tidemand-Lichtenberg, "500 nm continuous wave tunable single-frequency mid-IR light source for C-H spectroscopy," *Laser Phys.*, vol. 22, no. 11, pp. 1676–1681, 2012.

[4] K. Krzempek, G. Sobon, and K. M. Abramski, "DFG-based mid-IR generation using a compact dual-wavelength all-fiber amplifier for laser spectroscopy applications," *Opt. Express*, vol. 21, no. 17, pp. 20023–20031, 2013.

[5] H. Northern, S. O'Hagan, M. L. Hamilton, and P. Ewart, "Mid-infrared multi-mode absorption spectroscopy, MUMAS, using difference frequency generation," *Appl. Phys. B*, vol. 118, no. 3, pp. 343–351, 2015.

[6] N. Savage, "Optical parametric oscillators," *Nat. Photon.*, vol. 4, no. 283, pp. 124–125, 2010.

[7] X. Hong, X. Shen, M. Gong, and F. Wang, "Broadly tunable mode-hop-free mid-infrared light source with MgO:PPLN continuous-wave optical parametric oscillator," *Opt. Lett.*, vol. 37, no. 23, pp. 4982–4984, 2012.

[8] V. Kemlin *et al.*, "Widely tunable optical parametric oscillator in a 5 mm thick 5% MgO:PPLN partial cylinder," *Opt. Lett.*, vol. 38, no. 6, pp. 860–862, 2013.

[9] S. C. Kumar *et al.*, "High-power, widely tunable, room-temperature picosecond optical parametric oscillator based on cylindrical 5%MgO:PPLN," *Opt. Lett.*, vol. 40, no. 16, pp. 3897–3900, 2015.

[10] J. Liu *et al.*, "Highly efficient tunable mid-infrared optical parametric oscillator pumped by a wavelength locked, Q-switched Er:YAG laser," *Opt. Express*, vol. 23, no. 16, pp. 20812–20919, 2015.

[11] A. Hemming *et al.*, "99 W mid-IR operation of a ZGP OPO at 25% duty cycle," *Opt. Express*, vol. 21, no. 8, pp. 10062–10069, 2013.

[12] M. Vainio, M. Siltanen, J. Peltola, and L. Halonen, "Grating-cavity continuous-wave optical parametric oscillators for high-resolution mid-infrared spectroscopy," *Appl. Opt.*, vol. 50, no. 4, pp. A1–A10, 2011.

[13] I. Ricciardi *et al.*, "Sub-kilohertz linewidth narrowing of a mid-infrared optical parametric oscillator idler frequency by direct cavity stabilization," *Opt. Exp.*, vol. 40, no. 20, pp. 4743–4746, 2015.

[14] P. E. Powers, K. W. Aniolek, T. J. Kulp, B. A. Richman, and S. E. Bisson, "Periodically poled lithium niobate optical parametric amplifier seeded with the narrow-band filtered output of an optical parametric generator," *Opt. Lett.*, vol. 23, no. 24, pp. 1886–1888, 1998.

[15] L. Goldberg, W. K. Burns, and R. W. McElhanon, "Difference-frequency generation of tunable mid-infrared radiation in bulk periodically poled LiNbO3," *Opt. Lett.*, vol. 20, no. 11, pp. 1280–1282, 1995.

[16] Q. H. Mao, J. Jiang, X. Q. Li, J. H. Chang, and W. Q. Liu, "Widely tunable continuous wave mid-IR DFG source based on fiber lasers and amplifiers," *Laser Phys. Lett.*, vol. 6, no. 9, pp. 647–652, 2009.

[17] G. Shekhar, O. B. Jacob, and P. G. Leonel , "Multiwatt-level continuous-wave midwave infrared generation using difference frequency mixing in periodically poled MgO-doped lithium niobate," *Opt. Lett.*, vol. 39, no. 17, pp. 5018–5021, 2014.

[18] N. Polydorides, S. Tsekenis, H. McCann, V. Archilla Prat, and P. Wright, "An efficient approach for limited data chemical species tomography and its error bounds," *Proc. Roy. Soc. A, Math., Phys. Eng. Sci.*, vol. 472, no. 2187, 2016, Art. no. 20150875. doi: 10.1098/rspa.2015.0875

[19] P. Wright *et al.*, "Implementation of non-intrusive jet exhaust species distribution measurements within a test facility," in *Proc. 2016 IEEE Aerosp. Conf.*, 2016, pp. 1–14.

[20] P. Wright *et al.*, "Progress towards non-intrusive optical measurement of gas turbine exhaust species distributions," in *Proc. IEEE Aerosp. Conf.*, 2015, pp. 1–14.

[21] Y. Feng *et al.*, "LD-seeded thulium-doped fibre amplifier for CO2 measurements at 2 μm," in *Proc.6th Europhoton Conf.*, Neuchâtel, Switzerland, Aug. 2014, p. TuP-T1-P-12.

[22] [Online]. Available: http://www.flites.eu/. Accessed on: Jul. 27, 2017.

[23] J. Nilsson *et al.*, "High-power wavelength-tunable cladding-pumped rare-earth-doped silica fiber lasers," *Opt. Fiber Technol.*, vol. 10, no. 1, pp. 5–30, 2004.

[24] R. Royon, J. Lhermite, L. Sarger, and E. Cormier, "High power, continuous-wave ytterbium-doped fiber laser tunable from 976 to 1120 nm," *Opt. Express*, vol. 21, no. 11, pp. 13818–13823, 2013.

[25] Y. Sun *et al.*, "80 nm ultra-wideband erbium-doped silica fibre amplifier," *Electron. Lett.*, vol. 33, no. 23, pp. 1965–1967, 1997.

[26] V. Petrov, "Frequency down-conversion of solid-state laser sources to the mid-infrared spectral range using non-oxide nonlinear crystals," *Prog. Quant. Electron.*, vol. 42, pp. 1–106, 2015.

[27] [Online]. Available: https://www.covesion.com/support/covesion-guide-to-ppln/material-properties-of-lithium-niobate.html. Accessed on: Jul. 27, 2017.

[28] S. Guha, "Focusing dependence of the efficiency of a singly resonant optical parametric oscillator," *Appl. Phys. B*, vol. 66, no. 6, pp. 663–675, 1998.

[29] G. D. Boyd and D. A. Kleinman, "Parametric interaction of focused Gaussian light beams," *J. Appl. Phys.*, vol. 39, no. 8, pp. 3597–3639, 1968.

[30] Y. Jeong, J. K. Sahu, D. B. S. Soh, C. A. Codemard, and J. Nilsson, "High-power tunable single-frequency single-mode erbium:ytterbium co-doped large-core fiber master-oscillator power amplifier source," *Opt. Lett.*, vol. 30, no. 30, pp. 2997–2999, 2005.
[31] [Online]. Available: http://www.hcphotonics.com/products2.asp?area=1670&cat=1750&sn=1013. Accessed on: Jul. 27, 2017.
[32] R. T. Murray, T. H. Runcorn, E. J. R. Kelleher, and J. R. Taylor, "Highly efficient mid-infrared difference-frequency generation using synchronously pulsed fiber lasers," *Opt. Lett.*, vol. 41, no. 11, pp. 2446–2449, 2016.
[33] P. Belden, D. W. Chen, and F. D. Teodoro, "Watt-level, gigahertz-linewidth difference-frequency generation in PPLN pumped by an nanosecond-pulse fiber laser source," *Opt. Lett.*, vol. 40, no. 6, pp. 958–961, 2015.

Junqing Zhao received the B.S. degree in applied physics from Henan Polytechnic University, Jiaozuo, China, in 2009, and the Ph.D. degree in optical engineering from Shenzhen University, Shenzhen, China, in 2014. He joined the High Power Fibre Lasers Group at the Optoelectronics Research Centre (ORC), University of Southampton, UK, in 2015. His research interests include continuous wave and pulsed fiber lasers, high-power fiber lasers and amplifiers, mid-infrared laser generation via nonlinear optics technologies and components with active dopants, mid-infrared supercontinuum generation, and related applications.

Fuqiang Jia received the B.S. degree in optics from Changchun University of Science and Technology, Changchun, China, in 2002, and the Ph.D. degree in optics from Changchun Institute of Optics, Fine Mechanics and Physics, Chinese Academy of Science, Changchun, China in 2007. He is an Associate Professor at Xiamen University, Xiamen, China. He has been working in the Department of Electronic Engineering, Xiamen University, since July 2007. During December 2013 to December 2014 and August 2015 to September 2015, he worked at Optoelectronics Research Centre, University of Southampton, Southampton, U.K., as an Academic Visitor, funded by the Chinese Scholarship Council. His research interests include advanced solid state lasers, fiber lasers and amplifiers, laser systems, and applications aspects. He is an author or coauthor of more than 30 international journal and conference papers.

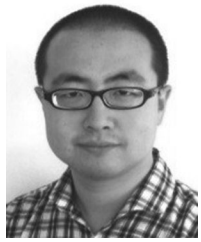

Yutong Feng received the B.S. degree in applied physics from Northwest University, Xi'an, China, in 2004, and the Ph.D. degree in optical engineering from Shanghai Institute of Optics and Fine Mechanics, Chinese Academy of Sciences, Beijing, China, in 2009. From 2009 to 2012, he was a Research Assistant at the North China Research Institute of Electro-Optics, Beijing. He is currently a Postdoctoral Research Fellow at the Optoelectronics Research Centre (ORC), University of Southampton, Southampton, U.K. His research interests include high power fiber lasers and amplifiers, nonlinear fiber optics, systems and applications.

Johan Nilsson received the Doctorate degree in engineering science from the Royal Institute of Technology, Stockholm, Sweden, for research on optical amplification, in 1994. He is a Professor at the ORC, University of Southampton, Southampton, U.K., and the Head of the High Power Fiber Lasers research group. Since 1994, he has been working on optical amplifiers and amplification in lightwave systems, optical communications, and guided-wave lasers, first at Samsung Electronics and later at ORC. His research has covered system, fabrication, and materials aspects, and in particular device aspects of high power fiber lasers, and erbium-doped fiber amplifiers. He has published some 400 scientific articles. He is a Fellow of the OSA and the SPIE, and a consultant to, and Co-Founder of, SPI Lasers. He is a member of the advisory board of the *Journal of the Optical Society of Korea* and was a Guest editor of two issues on high-power fiber lasers in the IEEE JOURNAL OF SELECTED TOPICS IN QUANTUM ELECTRONICS in 2009. He is a Former Chair of the Laser Science and Engineering technical group in OSA's Science and Engineering Council and is currently a Program Chair for the EuroPhoton and Advanced Solid State Lasers conferences.